Land-Surface Temperature Measurement from Space: Physical Principles and Inverse Modeling

ZHENGMING WAN AND JEFF DOZIER, MEMBER, IEEE

Abstract—**In order to apply the multiple-wavelength (split-window) method used for satellite measurement of sea-surface temperature from thermal-infrared data to land-surface temperatures, we statistically analyze simulations using an atmospheric radiative transfer model. The range of atmospheric conditions and surface temperatures simulated is wide enough to cover variations in clear atmospheric properties and surface temperatures, both of which are larger over land than over sea. Surface elevation is also included in the simulation as the most important topographic effect. Land covers characterized by measured or modeled spectral emissivities include snow, clay, sands, and tree leaf samples. The empirical inverse model can estimate the surface temperature with a standard deviation less than 0.3 K and a maximum error less than 1 K for viewing angles up to 40° from nadir under cloud-free conditions, given satellite measurements in three infrared channels. Bands from the NOAA AVHRR (Advanced Very High Resolution Radiometer) may be used, as can selected bands from sensors under consideration by EOSAT and NASA for future remote-sensing missions, either after the addition of multispectral thermal infrared channels to LandSAT or from a sensor with a wide field-of-view designed for measurements over land or sea (SeaWiFS). A band in the region from 10.2 to 11.0 μm will usually give the most reliable single-band estimate of surface temperature. In addition, a band in either the 3.5–4.0 μm region or in the 11.5–12.6 μm region must be included for accurate atmospheric correction, and a band below the ozone absorption feature at 9.6 μm (e.g., 8.2–8.8 μm) will increase the accuracy of the estimate of surface temperature.**

I. Introduction

REMOTE SENSING of ocean surface temperatures has been a primary function of satellite infrared radiometers since their inception, and there has been much research on atmospheric corrections to space-measured brightness temperatures and on detection of and corrections for cloud cover. In comparison, satellite remote sensing of land-surface temperatures is still primitive, even though the use of thermal-infrared measurements for analysis of land biophysical conditions has been under investigation for more than two decades [1]. The many possible applications include use of surface temperatures in climatology and meteorology [2], investigations in agriculture and natural vegetation [3], [4], determination of surficial geology [5], [6], soil moisture estimation [7]–[9], forest fire mapping [10], location of shallow aquifers [11], determination of surface wind fields [12], and estimation of snow surface energy flux [13], [14]. Some of the major research challenges are related to the removal from remotely sensed data of effects caused by atmospheric attenuation, surface emissivity, and topography [15], [16].

Land-surface temperature is one of the key parameters in the physics of land-surface processes on a regional as well as a global scale. It combines the results of all surface–atmosphere interactions and energy fluxes between the atmosphere and the ground [17], [18]. Therefore, the ability to accurately determine thermodynamic land-surface temperature is essential to many scientific problems and to the management of renewable resources [19]. With advances in thermal remote-sensing techniques and in computer capabilities, measurement of land-surface temperature from space allows investigations of surface climate at local, regional, and global scales.

Manuscript received July 13, 1988; revised October 27, 1988. This work was supported by the National Aeronautics and Space Administration under Grants NAS 5-28770 and NAG 5-917.

Z. Wan is with the Institute of Remote Sensing Applications, Academia Sinica, P.O. Box 775, Beijing, China.

J. Dozier is with the Center for Remote Sensing and Environmental Optics, University of California, Santa Barbara, Santa Barbara, CA 93106, and is also affiliated with the Jet Propulsion Laboratory, California Institute of Technology, Pasadena, CA 91109.

IEEE Log Number 8825561.

II. Measurement of Surface Temperature from Space

A. Sea-Surface Temperature

For determination of surface temperature, infrared measurements from aircraft or spacecraft are usually made in the wavelengths of an atmospheric window for which molecular absorption is small, generally between 10.5 and 11.5 μm or 10.5 and 12.5 μm, but also between 3.5 and 4.0 μm or the broader window from 8 to 14 μm. Even for clear atmospheric conditions, however, atmospheric absorption and emission in these windows are not negligible, and the problem is compounded when there are thick aerosols or thin clouds, which attenuate the signal from the surface but do not completely obscure it. Even for clear-sky conditions, the difference between surface temperature and satellite-measured brightness temperature from 10.5 to 12.5 μm can be as large as 10 K for tropical atmospheres.

For clear atmospheres, a useful and generally successful method for correcting atmospheric effects over the ocean surface combines infrared measurements in two or three wavelength bands. In the 10.5–11.5 μm window the principal absorbing agent is water vapor, whereas in the 3.5–4 μm window water vapor absorption is smaller, and absorption by nitrogen and other gases can be calculated

0196-2892/89/0500-0268$01.00 © 1989 IEEE

because their mixing ratios vary little. In the daytime, however, the signal in the 3.5–4 μm band is contaminated by reflected solar radiation. The average solar irradiance in this band is about eight times the emitted radiation from a blackbody at 300 K. An alternative, but similar, method instead splits the 10.5–12.5 μm band into two parts, and compares the signal from 10.5 to 11.5 μm to that from about 11.5 to 12.5 μm, where water vapor absorption is slightly greater. Therefore, the difference between the measurements in either the two distinct windows or the two parts of the split window can be used to account for water vapor absorption and determine the surface temperature, given that spectral surface emissivities in the wavelength bands are known [20]–[24].

Investigation of the validity of this approach can be pursued through simulation of infrared brightness temperatures above the atmosphere in two or three wavelength bands for a variety of atmospheric temperature and humidity profiles. A radiative transfer model calculates atmospheric absorption and emission, and the results of the simulations are analyzed to develop empirical corrections. This is the approach used operationally by NOAA's sea-surface temperature mapping program [24], [25]. Thus far, however, only absorption and emission have been considered, in that the atmospheric models used [26], [27] do not account for clouds or other atmospheric aerosols which both absorb and scatter infrared radiation.

For atmospheres with thin clouds, Chahine [28] has explored the use of the 4.3 and 15 μm atmospheric sounder frequencies (many narrow wavelength channels clustered in the two CO_2 absorption bands) to derive a vertical profile of the atmospheric temperature and humidity, which can then be used to estimate surface temperature. The main obstacle with using his approach is the difficulty in constructing and operating such a sounder at appropriate spatial resolution for land-surface temperature applications, because the wavelength bands are so narrow that the signal-to-noise ratio is very low unless the instantaneous field-of-view is large. However, the method works well for coarse spatial resolution [29].

B. Extending Methods for Sea-Surface Temperature to the Land Surface

Price [16] applied the same method for measuring ocean temperatures to the land surface, using the split-window channels of the NOAA-7 AVHRR. He found that variations in the spectral emissivity could produce large errors. In [19] was modeled a spectral band selection over a hypothetical sample population of 185 different kinds of materials, a temperature range of 35°C, and different atmospheric conditions. A linear correction function had a standard deviation of 3.66°C. Becker [30] has shown the impact of spectral emissivity on the measurement of land-surface temperature from satellites, by correcting for atmospheric effects using the split-window method. He derived a series of linear approximations and concluded that accurate knowledge of the surface spectral emissivity is needed to infer land-surface temperature from space.

These papers demonstrate that simple extension to the land surface of the methods developed for sea-surface temperature measurements would lead to unacceptable errors. There are several reasons.

1) Emissivity: There is considerable spectral variation in emissivity for different land-surface materials and, for many of them, emissivities have been measured only for the spectrally integrated range from 8 to 14 μm [31]. Emissivity may also vary with the viewing angle [14], an effect that is more important over land than over water because the combination of surface slope and satellite scan angle routinely results in local viewing angles greater than 60°. In vegetation, the emitted radiation varies with the viewing angle, but more because of temperature structure in the vegetation canopy than because of angular effects in the emissivity [32].

2) Temperature Variation: The lower thermal diffusivity for soils, compared to water, and the lower rates of evaporation cause a wider range in land-surface temperature than ocean-surface temperature.

3) Nonuniform Field-of-View: The "mixed-pixel" problem, whereby the field-of-view consists of surfaces of different temperatures or emissivities, is more common over land. The nonlinear response of the Planck function causes the brightness temperatures of such a pixel to vary with wavelength, even in the absence of an atmosphere [33], [34].

4) Atmospheric Profile Variation: Variation in atmospheric profiles over land is increased by topographic changes, and the boundary layer of the atmosphere is not so closely coupled to surface properties as it is over the ocean. Aerosols are also more prevalent over land.

C. Nature of the Inverse Problem

One of the basic questions in remote-sensing research concerns the relation between ground measurements and measurements from airplanes or satellites using equivalent radiometric detectors. It is obvious that there is more atmospheric effect on space measurements of surface temperature, although the atmosphere also affects ground measurements because the land surface reflects radiation emitted from the atmosphere. In order to get accurate land-surface temperature estimates from space, it is necessary to correct for both the atmosphere and spectral emissivity; that is, to find a method to use space-acquired measurements of brightness temperature to derive the desired quantity, the surface thermodynamic temperature.

An essential feature of the inverse problem is that it is a set of nonlinear integro-differential equations with a nonlinear boundary condition. Radiance is a nonlinear function of temperature, and the atmospheric transmission in each band is a nonlinear function of atmospheric composition.

The possibility of solution of the inverse problem varies with different physical situations. When the surface emissivities are known precisely, for example, for a water surface, then the determination of surface temperature under cloud-free conditions is not difficult. However, when

we deal with variable atmospheric conditions and land surfaces with variable spectral emissivities, the unknowns always outnumber the independent measurements of space radiance.

It is, therefore, not practical to try to find a direct method to measure land-surface temperature from space. Instead, it is possible to find a satisfactory solution, although not necessarily the best solution, by statistically analyzing a synthesized or experimental data set. But how should we derive the data set for statistical analysis? Pure experimental methods are impractical because it is difficult to synchronize field measurements with satellite overpasses and, also, because the wide variation in atmospheric conditions and land temperatures and emissivities cannot be covered in a field experiment. Instead, numerical modeling of the atmospheric radiative transfer process is an efficient and accurate way to provide useful synthetic data.

III. Physical Principles

A. Relations Between Emissivity and Brightness Temperature

Emitted spectral radiance L at wavelength λ from a surface at thermodynamic temperature T_s is given by multiplying spectral emissivity $\epsilon(\lambda)$ by the Planck function

$$L(\lambda, T) = \epsilon(\lambda)B(\lambda, T_s) = \epsilon(\lambda)\frac{2hc^2}{\lambda^5(e^{hc/k\lambda T_s} - 1)} \tag{1}$$

where $h = 6.63 \times 10^{-34}$ Js is Planck's constant, $c = 3 \times 10^8$ m/s is the velocity of light, $k = 1.38 \times 10^{-23}$ J/K is Boltzmann's constant, and λ is in meters.

The brightness temperature $T_b(\lambda)$ can be found by solving the Planck function for temperature, given the emitted spectral radiation. The brightness temperature at a given wavelength, emissivity, and temperature is, thus, the temperature of a blackbody that emits the same amount of radiation at that wavelength. The relationship between $T_b(\lambda)$, T_s, and $\epsilon(\lambda)$ is

$$T_s = \frac{hc}{k\lambda \ln(1 + \epsilon e^{hc/k\lambda T_b} - \epsilon)}. \tag{2}$$

Note that for $\epsilon(\lambda) = 1$ this reduces to the identity $T_s = T_b(\lambda)$.

A series approximation to the Planck equation is often used, whereupon e^x is replaced by its Taylor series $e^a[1 + (x - a) + (x - a)^2/2! + (x - a)^3/3! + \cdots]$. Setting a to zero and truncating this series at the first term yields the Rayleigh–Jeans approximation, commonly used in the microwave frequencies. In the thermal-infrared region, however, expanding the series around zero introduces large, possibly unacceptable errors. Instead, one can choose appropriate values of a for a particular wavelength-temperature region. Truncating the series expansion for the Planck function at the second order yields

$$B(\lambda, T_s) \simeq \frac{2hc^2}{\lambda^5(e^a - 1)} \cdot \left[1 - \left(\frac{hc}{k\lambda T_s} - a\right) + \frac{1}{2}\left(\frac{hc}{k\lambda T_s} - a\right)^2\right]. \tag{3}$$

Depending on the wavelength and temperature, the appropriate value of a is used, such that $a \simeq hc/k\lambda T_s$. The advantage of using such a series expansion is that the expression can usually be analytically integrated over, for example, a range of temperatures or wavelengths.

B. Radiative Transfer

The angular and azimuthal distribution of radiance at any level in an absorbing, emitting, and scattering layer is given by the radiative transfer equation [35]. For simplicity, the spectral designation is omitted from the equations that follow, but all quantities are monochromatic. Radiation from the sun and thermal radiation emitted from the earth and atmosphere are both considered:

$$\mu\frac{dL(\tau, \vec{\Omega})}{d\tau} + L(\tau, \vec{\Omega}) = J(\tau, \vec{\Omega}). \tag{4}$$

Here the sign convention is that the downward direction is positive. Optical depth is τ, increasing downward, and $L(\tau, \vec{\Omega})$ is the radiance at level τ along direction $\vec{\Omega}$, which is composed of zenith angle arc cos μ (downward positive) and azimuth ϕ. The source function J is

$$J(\tau, \vec{\Omega}) = \frac{\tilde{\omega}}{4\pi}\int_{4\pi} P(\tau, \vec{\Omega}; \vec{\Omega}')L(\tau, \vec{\Omega}')\,d\Omega' + Q(\tau, \vec{\Omega}). \tag{5}$$

The scattering phase function $P(\tau, \vec{\Omega}; \vec{\Omega}')$, calculated by rapid Mie algorithms [36], gives the distribution pattern of single scattering at τ caused by a pencil of radiation incident along direction $\vec{\Omega}'$ and scattered in direction $\vec{\Omega}$. The single scattering albedo is $\tilde{\omega}$. The first term on the right-hand side of (5) is then the total contribution made by radiation coming from all directions to the radiance at a particular direction $\vec{\Omega}$.

The Q term in (5) represents internal sources. By separating direct from diffuse radiation, it is convenient to consider the radiation scattered from the direct beam or the specularly reflected direct beam as caused by some internal "pseudo-source" [37]. Then, the total internal source is

$$Q(\tau, \vec{\Omega}) = Q_t(\tau, \vec{\Omega}) + Q_s(\tau, \vec{\Omega}) + Q_{sp}(\tau, \vec{\Omega}) \tag{6}$$

where Q_t is the thermal source and Q_s and Q_{sp} are the direct and specular pseudo-sources. Then

$$Q_t(\tau, \vec{\Omega}) = (1 - \tilde{\omega})B[T(\tau)] \tag{7}$$

$$Q_s(\tau, \vec{\Omega}) = \frac{\tilde{\omega}E_0}{4\pi}P(\tau, \vec{\Omega}; \vec{\Omega}_0)e^{-\tau/\mu_0} \tag{8}$$

$$Q_{sp}(\tau, \vec{\Omega}) = \frac{\tilde{\omega}E_0}{4\pi} R_{sp}(\mu_0) P(\tau, \vec{\Omega}; \vec{\Omega}_{sp}) e^{-(2\tau_0 - \tau)/\mu_0} \quad (9)$$

where $B[T(\tau)]$ is the Planck function, μ_0 is the cosine of the solar zenith angle, E_0 is the solar irradiance incident on the top of the atmosphere (normal to the beam), R_{sp} is the directional specular reflectivity at the surface beneath the atmosphere, and τ_0 is the total optical thickness of the atmosphere.

To resolve scattering phase functions with strongly forward peaks using a lower-order polynomial approximation, a delta-M transformation is performed for the phase function moments, optical depth, and single scattering albedo [38]. By applying the interaction principle [39] and doubling method [37], [40], a matrix form of this integro-differential, radiative transfer equation can be applied to a vertically inhomogeneous, multilayer atmosphere [41]. The top and bottom boundary conditions that need to be satisfied are that $\boldsymbol{L}^{\downarrow}(0)$ must be specified (usually zero) and

$$\boldsymbol{L}^{\uparrow}(\tau_0) = \boldsymbol{R}_g \boldsymbol{L}^{\downarrow}(\tau_0) + \vec{\epsilon} B(T_s) + \frac{\mu_0 E_0}{\pi} e^{-\tau_0/\mu_0} \boldsymbol{f}_r(\mu_0). \quad (10)$$

Radiances $\boldsymbol{L}^{\downarrow\uparrow}$ are vectors of $m \times n$ elements on a discrete angular space composed of m zenith and n azimuth angles

$$\boldsymbol{L}^{\downarrow\uparrow}(\tau) = \begin{bmatrix} L(\tau, \pm\mu_1, \phi_1) \\ L(\tau, \pm\mu_1, \phi_2) \\ \cdots\cdots \\ L(\tau, \pm\mu_m, \phi_n) \end{bmatrix} \quad (11)$$

where $1 \geq \mu_1 > \cdots > \mu_m > 0$ are a set of quadrature points on [0], [1], and $0 \leq \phi_1 < \cdots < \phi_n < 2\pi$ are equally spaced points on the interval $[0, 2\pi]$. Also, $\boldsymbol{R}_g$ is the surface diffuse reflection matrix, T_s is the temperature of the surface, $\boldsymbol{f}_r(\mu_0)$ is the surface BRDF (bidirectional reflectance-distribution function) vector to the direct beam, and $\vec{\epsilon}$ is the emissivity vector. The directional emissivity and BRDF f_r are coupled by Kirchhoff's law

$$\epsilon(\mu) = 1 - \int_0^{2\pi} \int_0^1 \mu' f_r(\mu; \mu', \phi')\, d\mu'\, d\phi'. \quad (12)$$

C. Incorporation of LOWTRAN Calculations

As described thus far, the model is for the monochromatic case only. To make the model work for the atmosphere, we need to know the atmospheric optical properties: optical thickness τ_0, single scattering albedo $\tilde{\omega}$, and scattering phase function P.

Given an atmospheric profile (temperature, pressure, water vapor denisty, ozone density, and aerosol density and distribution) the LOWTRAN codes [27] and Mie-scattering calculations [36] give the atmospheric transmittance profile for wavelengths from 0.25 to 28.5 μm, averaged over every 20 cm^{-1} wavenumber interval. Thus, LOWTRAN does not really give monochromatic transmittance. This averaging causes violation of the Lambert–Bouguer–Beer law because of the complexity of molecular band absorption even in a narrow wavenumber interval like 20 cm^{-1}, equivalent to $\Delta\lambda = 27$ nm at $\lambda = 3.7$ μm, and to $\Delta\lambda = 242$ nm at $\lambda = 11$ μm. A solution to this problem is to expand radiative transmission functions calculated from LOWTRAN by using "exponential-sum fitting" [42]. The monochromatic radiative transfer model is applied separately to each term in the exponential-sum expansion, and the results are then summed. By solving the radiative transfer equation over the whole wavelength range of a thermal band of a satellite sensor, we get the angular distribution vector of average spectral radiance. The term Ψ is the sensor response function for the wavelength band whose lower and upper boundaries are $[\lambda_1, \lambda_2]$

$$\overline{\boldsymbol{L}^{\uparrow}} = \frac{\int_{\lambda_1}^{\lambda_2} \Psi(\lambda) \boldsymbol{L}^{\uparrow}(\lambda, 0)\, d\lambda}{\int_{\lambda_1}^{\lambda_2} \Psi(\lambda)\, d\lambda}. \quad (13)$$

D. Simplification of the Lower Boundary Condition

The bottom boundary condition described in (10) represents a static interface, in the thermal-infrared region, to an energy balance model of the land-surface processes. The spectral emissivity may change as a result of land-surface processes. Physical and chemical changes in the surface material (for example, a change in moisture conditions) will change emissivity, as will morphological changes in the system (for example, geometric changes in a vegetation canopy). Therefore, field measurement of spectral emissivity is usually difficult, and apparent values often depend on experimental arrangements.

In daylight, the satellite sensor receives sunlight scattered by the atmosphere and reflected by the land surface. Inclusion of the middle-infrared wavelength region (3.5–4.0 μm) increases our difficulty because unless $\vec{\epsilon}$ is known it is impossible to separate emitted from reflected radiance. We, therefore, drop terms relevant to the sunlight in all the above equations by avoiding use of the middle-infrared region in daylight. Then the radiative transfer equation is azimuthally independent, and the bottom boundary condition becomes, in integral form

$$L(\lambda, \tau_0, -\mu) = 2\pi \int_0^1 \mu' f_r(\lambda, -\mu, \mu') L(\lambda, \tau_0, \mu') \cdot d\mu' + \epsilon(\lambda, -\mu) b(\lambda, T_s). \quad (14)$$

Although there is ample evidence that the emissivities of land surfaces such as soils, sands, and vegetation canopies vary with the viewing angle [32], [43]–[46], there are little such spectral, angular emissivity data available. Therefore, we assume that land surfaces are Lambertian, so emissivity is independent of viewing angle. This approximation is usually not too bad for viewing angles up

to about 40° from nadir. Kirchhoff's law (12) then becomes

$$\epsilon(\lambda) = 1 - R(\lambda) \tag{15}$$

where $\epsilon(\lambda)$ is the spectral emissivity and $R(\lambda)$ is the spectral reflectance, which equals πf_r under the Lambertian assumption. The bottom boundary condition (10) then takes the simple form

$$L(\lambda, \tau_0, -\mu) = \epsilon(\lambda)B(\lambda, T_s) + 2[1 - \epsilon(\lambda)] \cdot \int_0^1 \mu' L(\lambda, \tau_0, \mu')\, d\mu'. \tag{16}$$

This equation provides a relationship between spectral emissivity and temperature. Unfortunately, it also contains the integral of downward radiance at the surface, so it is used as a boundary condition for solving the radiative transfer equation rather than as an extra relationship for finding a deterministic solution to the inverse problem.

IV. Numerical Modeling of the Forward Problem

The range of atmospheric and surface conditions considered in the model, shown in Table I, is wider than the realistic regime so that the resulting statistical model will cover actual situations. We discuss the variation of parameters first and then show some results from the atmospheric model.

A. Atmospheric Conditions

As shown in Table I, we use five "standard" atmospheric profiles whose properties are incorporated into the LOWTRAN code:

U.S. standard
mid-latitude spring/summer
mid-latitude fall/winter
subarctic spring/summer
subarctic fall/winter.

A combination of these atmospheres represents most of the northern hemisphere through the seasons. A rural aerosol distribution used in LOWTRAN applies to all these atmospheric profiles in the elevation range from 0 to 9 km, with visibilities near the earth's surface either 10 or 23 km. In the elevation range from 10 to 30 km is the background stratospheric aerosol; above that is the normal upper atmospheric aerosol.

B. Surface Conditions

The surface conditions are also summarized in Table I. For temperatures less than 273 K, we use a deep snow layer composed of spherical ice particles with a radius of 250 μm. The snow layer's emissivity and phase function are calculated from the same radiative transfer model that we use for the atmosphere. For higher temperatures, we consider a range of surfaces—tree leaf, clay, coarse sand, and fine sand—and use measured values for their spectral emissivities [46], [47], as shown in Fig. 1. The surface temperature varies within ±20 K around the air temperature at the lower boundary of the atmospheric profile in use. The surface elevations considered are 0, 0.25, 0.5, 0.75, 1, 2, 3, 4, and 6 km.

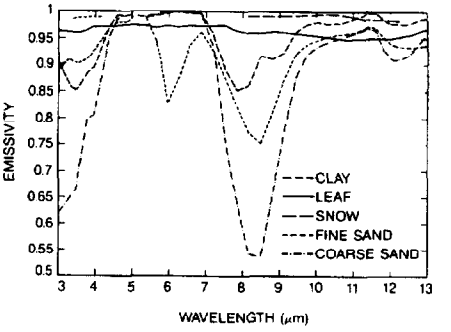

Fig. 1. Spectral emissivity of land surfaces.

TABLE I
RANGE OF CONDITIONS IN SIMULATION

atmosphere	surface visibility (km)	air temperature (°K)	land cover	surface elevation (km)	surface temperature (°K)
U.S. standard	10	288.2	leaf, clay, sands	0	268-308
U.S. standard	10	288.2	snow	0	258-273
U.S. standard	23	288.2	leaf, clay, sands	0	268-308
U.S. standard	23	288.2	snow	0	258-273
summer mid-lat	23	294.2	leaf, clay, sands	0, 0.25, 0.5, 0.75, 1, 2, 3, 4	240-313
summer mid-lat	23	294.2	snow	0, 0.25, 0.5, 0.75, 1, 2, 3, 4, 6	240-273
winter mid-lat	23	272.1	leaf, clay, sands	0, 1, 2, 3, 4	235-293
winter mid-lat	23	272.1	snow	0, 1, 2, 3, 4	230-273
summer subarctic	23	287.2	leaf, clay, sands	0	265-305
summer subarctic	23	287.2	snow	0	250-273
winter subarctic	23	257.1	leaf, clay, sands	0	235-275
winter subarctic	23	257.1	snow	0	230-260

C. Sensor Spectral Specification

Three sensors are considered: the NOAA AVHRR with three thermal bands, and two sensors based on reports of joint EOSAT/NASA working groups [19], [48]—a proposed multispectral thermal-infrared addition to the LandSAT Thematic Mapper (TM) and a wide field-of-view sensor for oceanic investigations (SeaWiFS). The wavelength bands of these three sensors are given in Table II. The proposed additional thermal wavelength bands for the TM do not include a band beyond 12 μm, which we have found important for atmospheric correction. Therefore, we include an additional sixth band in the TM calculations, as shown in Table II. For the NOAA AVHRR, the actual sensor response functions (from NOAA-9) are used. For the hypothetical instruments we consider an idealized trapezoidal response function

$$\lambda_1 + \delta\lambda \le \lambda \le \lambda_2 - \delta\lambda \quad \Psi(\lambda) = 1$$

$$\lambda_1 < \lambda < \lambda_1 + \delta\lambda \quad \Psi(\lambda) = \frac{\lambda - \lambda_1}{\delta\lambda}$$

$$\lambda_2 > \lambda > \lambda_2 + \delta\lambda \quad \Psi(\lambda) = \frac{\lambda_2 - \lambda}{\delta\lambda}$$

$$\lambda \ge \lambda_2 \text{ or } \lambda \le \lambda_1 \quad \Psi(\lambda) = 0$$

$$Q_{sp}(\tau, \vec{\Omega}) = \frac{\tilde{\omega}E_0}{4\pi} R_{sp}(\mu_0) P(\tau, \vec{\Omega}; \vec{\Omega}_{sp}) e^{-(2\tau_0 - \tau)/\mu_0} \quad (9)$$

where $B[T(\tau)]$ is the Planck function, μ_0 is the cosine of the solar zenith angle, E_0 is the solar irradiance incident on the top of the atmosphere (normal to the beam), R_{sp} is the directional specular reflectivity at the surface beneath the atmosphere, and τ_0 is the total optical thickness of the atmosphere.

To resolve scattering phase functions with strongly forward peaks using a lower-order polynomial approximation, a delta-M transformation is performed for the phase function moments, optical depth, and single scattering albedo [38]. By applying the interaction principle [39] and doubling method [37], [40], a matrix form of this integro-differential, radiative transfer equation can be applied to a vertically inhomogeneous, multilayer atmosphere [41]. The top and bottom boundary conditions that need to be satisfied are that $\boldsymbol{L}^{\downarrow}(0)$ must be specified (usually zero) and

$$\boldsymbol{L}^{\uparrow}(\tau_0) = \boldsymbol{R}_g \boldsymbol{L}^{\downarrow}(\tau_0) + \vec{\epsilon} B(T_s) + \frac{\mu_0 E_0}{\pi} e^{-\tau_0/\mu_0} \boldsymbol{f}_r(\mu_0). \quad (10)$$

Radiances $\boldsymbol{L}^{\downarrow\uparrow}$ are vectors of $m \times n$ elements on a discrete angular space composed of m zenith and n azimuth angles

$$\boldsymbol{L}^{\downarrow\uparrow}(\tau) = \begin{bmatrix} L(\tau, \pm\mu_1, \phi_1) \\ L(\tau, \pm\mu_1, \phi_2) \\ \cdots\cdots \\ L(\tau, \pm\mu_m, \phi_n) \end{bmatrix} \quad (11)$$

where $1 \geq \mu_1 > \cdots > \mu_m > 0$ are a set of quadrature points on [0], [1], and $0 \leq \phi_1 < \cdots < \phi_n < 2\pi$ are equally spaced points on the interval $[0, 2\pi]$. Also, $\boldsymbol{R}_g$ is the surface diffuse reflection matrix, T_s is the temperature of the surface, $\boldsymbol{f}_r(\mu_0)$ is the surface BRDF (bidirectional reflectance-distribution function) vector to the direct beam, and $\vec{\epsilon}$ is the emissivity vector. The directional emissivity and BRDF f_r are coupled by Kirchhoff's law

$$\epsilon(\mu) = 1 - \int_0^{2\pi} \int_0^1 \mu' f_r(\mu; \mu', \phi')\, d\mu'\, d\phi'. \quad (12)$$

C. Incorporation of LOWTRAN Calculations

As described thus far, the model is for the monochromatic case only. To make the model work for the atmosphere, we need to know the atmospheric optical properties: optical thickness τ_0, single scattering albedo $\tilde{\omega}$, and scattering phase function P.

Given an atmospheric profile (temperature, pressure, water vapor denisty, ozone density, and aerosol density and distribution) the LOWTRAN codes [27] and Mie-scattering calculations [36] give the atmospheric transmittance profile for wavelengths from 0.25 to 28.5 μm, averaged over every 20 cm^{-1} wavenumber interval. Thus, LOWTRAN does not really give monochromatic transmittance. This averaging causes violation of the Lambert–Bouguer–Beer law because of the complexity of molecular band absorption even in a narrow wavenumber interval like 20 cm^{-1}, equivalent to $\Delta\lambda = 27$ nm at $\lambda = 3.7$ μm, and to $\Delta\lambda = 242$ nm at $\lambda = 11$ μm. A solution to this problem is to expand radiative transmission functions calculated from LOWTRAN by using "exponential-sum fitting" [42]. The monochromatic radiative transfer model is applied separately to each term in the exponential-sum expansion, and the results are then summed. By solving the radiative transfer equation over the whole wavelength range of a thermal band of a satellite sensor, we get the angular distribution vector of average spectral radiance. The term Ψ is the sensor response function for the wavelength band whose lower and upper boundaries are $[\lambda_1, \lambda_2]$

$$\overline{\boldsymbol{L}^{\uparrow}} = \frac{\int_{\lambda_1}^{\lambda_2} \Psi(\lambda) \boldsymbol{L}^{\uparrow}(\lambda, 0)\, d\lambda}{\int_{\lambda_1}^{\lambda_2} \Psi(\lambda)\, d\lambda}. \quad (13)$$

D. Simplification of the Lower Boundary Condition

The bottom boundary condition described in (10) represents a static interface, in the thermal-infrared region, to an energy balance model of the land-surface processes. The spectral emissivity may change as a result of land-surface processes. Physical and chemical changes in the surface material (for example, a change in moisture conditions) will change emissivity, as will morphological changes in the system (for example, geometric changes in a vegetation canopy). Therefore, field measurement of spectral emissivity is usually difficult, and apparent values often depend on experimental arrangements.

In daylight, the satellite sensor receives sunlight scattered by the atmosphere and reflected by the land surface. Inclusion of the middle-infrared wavelength region (3.5–4.0 μm) increases our difficulty because unless $\vec{\epsilon}$ is known it is impossible to separate emitted from reflected radiance. We, therefore, drop terms relevant to the sunlight in all the above equations by avoiding use of the middle-infrared region in daylight. Then the radiative transfer equation is azimuthally independent, and the bottom boundary condition becomes, in integral form

$$L(\lambda, \tau_0, -\mu) = 2\pi \int_0^1 \mu' f_r(\lambda, -\mu, \mu') L(\lambda, \tau_0, \mu') \cdot d\mu' + \epsilon(\lambda, -\mu) b(\lambda, T_s). \quad (14)$$

Although there is ample evidence that the emissivities of land surfaces such as soils, sands, and vegetation canopies vary with the viewing angle [32], [43]–[46], there are little such spectral, angular emissivity data available. Therefore, we assume that land surfaces are Lambertian, so emissivity is independent of viewing angle. This approximation is usually not too bad for viewing angles up

surements were wrong by about 2 K after the 1982 El Chichón eruption placed large amounts of sulfur-aerosols in the stratosphere [50], [51].

Because of the difficulties discussed earlier in Section II-B and II-C, we resort to a more complicated regression form than is used in the multiple-window sea-surface temperature technique. The second-order effects are large enough to be considered. The data set to be analyzed consists of results at the first four Gaussian nadir angles (up to 53.7°) to ensure that the resulting model gives good estimates for angles up to 45°.

A. Application to NOAA AVHRR Data

The standard errors in surface temperature for several combinations of bands from the NOAA AVHRR are shown in Table III. As verified experimentally for the ocean [52] and for all land covers in this study, the split window in the 10.3–12.4 μm region gives better results than a pair of windows in two separate regions of the spectrum. However, the two-window method is not good enough to make both atmospheric and emissivity correction for land surfaces that have more features in their emission spectra. The triple-band method gives accurate estimates of surface temperatures for snow, clay, tree leaf, and even for coarse sand, which has strong spectral emissivity features. The standard deviations of the surface temperature are less than 0.25 K and maximum errors are less than 1 K for viewing angles up to more than 50° under all cloud-free atmospheric conditions in our simulation and for the wide range of surface temperatures shown in Table I. It is possible to find a common formula that gives accurate estimates for more than one kind of land surface if the surfaces have similar spectral emissivities, as shown in the last column of Table III, where the same equation was used for snow and tree leaves. But this is not the case for arbitrary spectral variation in emissivity.

B. Hypothetical Bands

In the report of the joint EOSAT/NASA thermal-infrared working group [19], a five-band thermal instrument, with bandpasses as shown in Table II, was proposed for the future LandSAT-7 platform. Our simulation shows that bands 4 and 5 of this sensor, the split-window in the 10–13 μm region, are not suitably designed for atmospheric correction. The primary motivation for locating these bands was for spectral discrimination of some of the silicate minerals. The atmospheric effects in these two bands are very similar, as shown in Figs. 2 and 3. Therefore, we add a band at 11.8–12.6 μm, which is similar to the fifth band in the "second-priority" recommendations in the same report [19]. In the following, we examine this hypothetical six-band thermal instrument. The same analyses can be applied to the proposed SeaWiFS instrument [48] because of the similarity of the most useful bands for atmospheric correction.

TABLE III
STANDARD DEVIATIONS IN LINEAR AND QUADRATIC REGRESSION MODELS FOR LAND-SURFACE TEMPERATURE FROM THREE NOAA AVHRR THERMAL BANDS ($\theta \leq 53.7°$)

bands used	snow		coarse sands		clay		tree leaf		snow and leaf	
	linear (°K)	quad. (°K)	linear (°K)	quad. (°K)	linear (°K)	quad. (°K)	linear (°K)	quad. (°K)	linear (°K)	quad. (°K)
4-3	1.22	0.881	-	1.021	-	0.701	0.560	0.423	-	-
4-5	0.29	0.193	-	0.471	-	0.240	0.425	0.257	-	-
4-5-3	-	0.138	0.280	0.194	0.268	0.205	0.268	0.172	0.441	0.360

C. Known Emissivities

Assuming that we know spectral emissivity values for the land surface whose temperature is needed, we find a simple but general model to estimate the temperature for these surfaces, and then analyze its sensitivity to emissivity errors. Because the emissivity is directly related to radiance rather than to temperature, a radiance model is preferred to a temperature model. That is, we try to estimate the radiance L_s emitted from the surface from which we can calculate the surface temperature.

First of all, we define band-averaged emissivity as

$$\overline{\epsilon(T_s)} = \frac{\int_{\lambda_1}^{\lambda_2} \Psi(\lambda)\epsilon(\lambda)B(\lambda, T_s)\, d\lambda}{\int_{\lambda_1}^{\lambda_2} \Psi(\lambda)B(\lambda, T_s)\, d\lambda} \tag{17}$$

where Ψ is the sensor response function, $\epsilon(\lambda)$ is the spectral emissivity, $B(\lambda, T_s)$ is the Planck function, and λ_1 and λ_2 are the lower and upper boundaries of the band. The band-averaged emissivity varies only weakly with temperature, and we ignore this small dependence here.

The subscripts on radiance L and emissivity ϵ in the equations that follow refer to the bands from Table II. We will use the relation L/ϵ as a first-order emissivity correction, and correct for the atmosphere with a regression method, where μ is the cosine of the viewing angle from zenith as measured at the surface. Our simulation data set of 2128 situations includes various atmospheric profiles and surface temperatures, and surfaces composed of tree leaves, clay, snow, fine sands, coarse sands, and mixed sands. Two emissivity-radiance models are obtained from statistical analysis of the simulations: one using LandSAT thermal bands 4, 1, and 6, and the other with bands 4, 2, and 6. Each gives the blackbody radiance in band 4, corrected for atmosphere and emissivity.

The LandSAT thermal band 4-1-6 model is

$$L_{s,4}(4, 1, 6) = (0.1048L_1 - 0.098L_6)\,\mu^{-1} + \left(\frac{L_1}{\epsilon_1} - \frac{L_4}{\epsilon_4}\right) \times \left\{\left[0.0243\left(\frac{L_6}{\epsilon_6} - \frac{L_4}{\epsilon_4}\right) + 0.0237\right] \cdot \mu^{-1} - \frac{0.4226}{L_1} + 0.3513\right\} - \left(\frac{L_6}{\epsilon_6} - \frac{L_4}{\epsilon_4}\right) \cdot \left[0.3031\left(\frac{L_6}{\epsilon_6} - \frac{L_4}{\epsilon_4}\right) + \frac{7.0186}{L_6}\right.$$

$$- 0.1509\Big] + \left(\frac{0.2255}{\epsilon_6} - 0.229\right)L_6 + 0.2859L_4 + 0.7411L_1 - 0.096 \quad (18)$$

and the band 4-2-6 model is

$$L_{s,4}(4, 2, 6) = -(0.6359L_6 - 0.5743L_4 - 0.0867L_2)\mu^{-1} + \left(\frac{L_6}{\epsilon_6} - \frac{L_4}{\epsilon_4}\right) \cdot \left[-0.3183\left(\frac{L_6}{\epsilon_6} - \frac{L_4}{\epsilon_4}\right) + \frac{1.6766}{L_6} - 1.5142\right] - \left(\frac{L_2}{\epsilon_2} - \frac{L_4}{\epsilon_4}\right)\left[0.0104 \cdot \left(\frac{L_2}{\epsilon_2} - \frac{L_4}{\epsilon_4}\right) + \frac{0.2525}{L_2}\right] + \left(\frac{0.5262}{\epsilon_4} + 0.2696\right)L_4 + \left(\frac{0.1654}{\epsilon_2} + 0.05\right)L_2 - 0.056. \quad (19)$$

Table IV shows standard errors of these two models for land-surface temperature estimates from space. The top row of the table shows the error distributions of surface temperatures, as does Fig. 5.

D. Models With Uncertain Emissivities

The effect of the emissivity uncertainty on the accuracy of surface temperature is also given in Table IV. Although the methods using Landsat thermal bands 4-1-6 and 4-2-6 give almost the same accuracy when we know the emissivity, the band 4-1-6 model is less sensitive to the same uncertainty in emissivity. In either case, however, the error in temperature associated with a 0.01 uncertainty in spectral emissivity is larger than the error in the atmospheric correction model. If we include more high-order terms in the regression model, we can halve the error for the case where we know precise emissivity values for each band. But the equations are lengthy, so we do not list them here. Moreover, they offer no advantage over the simpler equations in their sensitivity to uncertainty in emissivity.

When we do not know the emissivity of the land surfaces we need to correct for atmospheric and emissivity variations at the same time, but this is impossible without some assumptions about the spectral variation in emissivity. As described thus far, statistical analysis is made separately for each land surface. In general, it is reasonable to classify remotely sensed data before making quantitative interpretations, but at this time there are few accurate data on spectral emissivity for many land covers. This is a fundamental block to the accurate measurement of land-surface temperature.

We can focus, however, on broad categories of emissivity variation, and assume that thermal data are combined with other remotely sensed data to classify the surface into broad categories. We separate the five land surfaces—clay, fine sands, coarse sands, tree leaf, and snow—into two groups. Group 1 includes clay and sands and represents surfaces with spectral emissivity features. Group 2 includes tree leaves and snow and represents spectrally flat surfaces. We developed a regression analysis to analyze results within each group. The resulting equations involve a quadratic expression of four thermal bands and thus contain more than 30 terms, so they are not presented here. However, they contain no explicit emissivity terms. For these two groups, the inverse models estimate surface temperature to a standard error of around 0.2 K, except for viewing angles exceeding 50°, as shown in Table V. Maximum errors are less than 1 K.

In this example of emissivity variation our approach to land-surface temperature measurement from thermal satellite data shows the ability to adapt to changes in atmospheric conditions, land-surface temperature, viewing an-

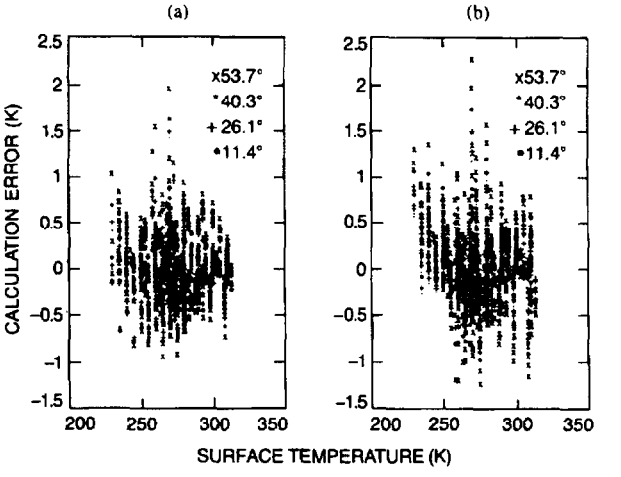

Fig. 5. Land-surface temperature errors in the radiance-emissivity model: (a) for LandSAT thermal bands 4-1-6; (b) for LandSAT thermal bands 4-2-6. Note that the vertical axis is stretched.

TABLE IV
DEPENDENCE OF RMS AND MAXIMUM ERROR OF LAND-SURFACE TEMPERATURE ON VIEWING ANGLE AND EMISSIVITY ERROR FOR LANDSAT THERMAL BANDS

bands used	variation in ϵ_j		rms ΔT_s (°K) (11.4°)	(26.1°)	(40.3°)	(53.7°)	max ΔT_s (°K) (11.4°)	(26.1°)	(40.3°)	(53.7°)
4-1-6	0.00		0.28	0.29	0.32	0.37	1.42	1.48	1.61	1.95
	+0.01	$j=1,4,6$	0.32	0.33	0.36	0.41	1.28	1.34	1.48	1.81
	-0.01	$j=1,4,6$	0.32	0.33	0.35	0.40	1.56	1.62	1.76	2.09
	+0.01	$j=1$	0.35	0.36	0.39	0.43	1.20	1.25	1.39	1.71
	-0.01	$j=1$	0.36	0.36	0.38	0.44	1.64	1.70	1.85	2.19
	+0.01	$j=4$	0.53	0.54	0.55	0.58	1.61	1.61	1.61	1.58
	-0.01	$j=4$	0.55	0.55	0.56	0.60	1.87	1.93	2.07	2.39
	+0.01	$j=6$	0.58	0.59	0.60	0.64	1.95	2.01	2.15	2.48
	-0.01	$j=6$	0.61	0.62	0.63	0.66	1.63	1.63	1.62	1.60
4-2-6	0.00		0.27	0.29	0.35	0.48	1.39	1.50	1.73	2.26
	+0.01	$j=2,4,6$	0.47	0.48	0.51	0.61	1.16	1.23	1.38	1.87
	-0.01	$j=2,4,6$	0.49	0.50	0.54	0.63	1.78	1.89	2.12	2.66
	+0.01	$j=2$	0.28	0.31	0.36	0.48	1.31	1.42	1.65	2.18
	-0.01	$j=2$	0.28	0.30	0.36	0.48	1.47	1.58	1.81	2.34
	+0.01	$j=4$	1.08	1.08	1.09	1.13	1.84	1.90	2.02	2.25
	-0.01	$j=4$	1.09	1.10	1.11	1.16	2.67	2.79	3.04	2.59
	+0.01	$j=6$	0.77	0.78	0.80	0.87	2.34	2.46	2.71	3.25
	-0.01	$j=6$	0.82	0.82	0.85	0.91	1.48	1.54	1.75	2.19

TABLE V
DEPENDENCE OF RMS AND MAXIMUM ERROR OF LAND-SURFACE TEMPERATURE ON VIEWING ANGLE IN GROUP MODELS (LANDSAT THERMAL BANDS 4-1-2-6)

surfaces	rms ΔT_s (°K) (11.4°)	(26.1°)	(40.3°)	(53.7°)	max ΔT_s (°K) (11.4°)	(26.1°)	(40.3°)	(53.7°)
Group 1 Model								
leaf	0.07	0.06	0.06	0.08	0.19	0.17	0.20	0.27
snow	0.09	0.10	0.11	0.14	0.45	0.48	0.55	0.69
Group 2 Model								
clay	0.13	0.14	0.17	0.25	0.37	0.41	0.50	0.70
sands	0.17	0.18	0.22	0.31	0.61	0.61	0.65	0.91

TABLE VI
EFFECT OF SATELLITE TEMPERATURE PRECISION ON ACCURACY OF CALCULATED LAND-SURFACE TEMPERATURE T_s

precision (°K)	rms ΔT_s (°K) (11.4°)	(26.1°)	(40.3°)	(53.7°)	max ΔT_s (°K) (11.4°)	(26.1°)	(40.3°)	(53.7°)
0.10	0.22	0.19	0.25	0.32	0.7	0.7	0.8	0.9
0.20	0.29	0.26	0.30	0.40	0.8	0.7	0.9	1.1
0.33	0.41	0.40	0.45	0.47	0.9	0.9	1.0	1.2
0.50	0.55	0.61	0.59	0.61	1.3	1.4	1.6	1.6

gle, and emissivity. The relationship between emissivity and radiance is linear, and the relationship between temperature and radiance is linear for small temperature changes. Thus, an accurate estimate of land-surface temperature is possible for surfaces with varied emissivity, provided atmospheric effects are corrected by the multiband method.

VI. SENSITIVITY OF THE MODEL

A. Sensitivity of the Statistical Inverse Model to the Data Set

The inverse model that we have developed is a skeleton for a statistical approach, based on a physical model, with a wide range of physical conditions in the synthesized data set. Therefore the solution is not unique. The parameters in the inverse model may change significantly when some simulated conditions are added into or dropped from the data set. Therefore the region of the model space was made wide enough to cover as much variation in the physical system as is feasible. An inverse model obtained statistically from a data set, which includes only a small variation of some parameter, may be sensitive to a small change of this parameter. Moreover, statistical models usually cannot predict or extrapolate.

B. Precision Requirements for Space Radiance Measurement

For simplicity in this section, we use brightness temperature at the satellite to represent the corresponding satellite-measured radiance for each band, but we must keep in mind that the quantization of the signal is linear in radiance, not in temperature. We round temperature values to the nearest 0.1 K, 0.2 K, 0.33 K, and 0.5 K, and we refer to these as the quantization precision. Table VI shows the standard deviation and maximum error for different viewing angles, for a sand surface, as functions of the precision. The inverse model developed in this study is tolerant of signal noise, calibration errors, and radiance-temperature transformation for each band, as long as the accuracy of the space-measured brightness temperature is better than 0.33 K. When we consider the variability and difficulty in land-surface temperature measurements, we recommend an effective temperature precision of 0.2 K.

VII. CONCLUSION

From this study, we have gained the following insights into the measurement of land-surface temperature from satellites:

1) It is a nonlinear problem, so linear approximations need to be cautiously evaluated.

2) Numerical modeling of atmospheric radiative transfer is an efficient and accurate way to simulate the physics of the satellite measurement of land-surface temperature.

3) Statistical inverse models may be derived from theoretical results of carefully designed numerical modeling, which spans the range of variations in the problem.

4) A band in the region from 11.8 to 12.6 μm is extremely useful for atmospheric correction; its specific location and bandwidth need to be investigated further.

5) It is possible to simultaneously make atmospheric correction and emissivity correction by using multiple wavelength thermal-infrared data from space, in order to get accurate estimates of surface temperatures of different land covers.

ACKNOWLEDGMENT

We thank J. C. Price, S. N. Goward, and an anonymous reviewer for helpful comments. Reference herein to any specific commercial product, process, or service by trade name, trademark, manufacturer, or otherwise, does not constitute or imply its endorsement by the United States Government, the University of California, Santa Barbara, or the Jet Propulsion Laboratory, California Institute of Technology.

REFERENCES

[1] M. Fuchs and C. B. Tanner, "Infrared thermometry of vegetation," *Agron. J.*, vol. 58, pp. 597-601, 1966.
[2] P. B. Francis, "Climate, oceans, and remote sensing," *Oceanus*, vol. 24, pp. 49-55, 1981.
[3] P. A. Murtha, "Frost pockets on thermal imagery," *Forest Chron.*, vol. 47, pp. 79-81, 1971.
[4] R. D. Jackson, R. J. Reginato, and S. B. Idso, "Wheat canopy temperature: A practical tool for evaluating water requirements," *Water Resour. Res.*, vol. 13, pp. 651-658, 1977.
[5] K. Watson, "Regional thermal inertia mapping from an experimental satellite," *Geophysics*, vol. 47, no. 12, pp. 1681-1687, 1982.
[6] A. B. Kahle, "Surface emittance, temperature, and thermal inertia derived from Thermal Infrared Multispectral Scanner (TIMS) data for Death Valley, California," *Geophysics*, vol. 52, no. 7, pp. 858-874, 1987.
[7] S. B. Idso, T. J. Schmugge, R. D. Jackson, and R. J. Reginato, "The utility of surface temperature measurements for the remote sensing of surface soil water status," *J. Geophys. Res.*, vol. 80, pp. 3044-3048, 1975.
[8] A. Rosema, "Simulation of the thermal behavior of bare soil for remote sensing purposes," in *Heat and Mass Transfer in the Biosphere, I, Transfer Processes in the Plant Environment*, D. A. de Vries and N. H. Afgan, Eds. Washington, DC: Scripta, 1975, pp. 109-123.
[9] J. C. Price, "The potential of remotely sensed thermal infrared data

to infer surface soil moisture and evaporation," *Water Resour. Res.*, vol. 16, no. 4, pp. 787-795, 1980.
[10] M. Matson, S. R. Schneider, B. Aldridge, and B. Satchwell, "Fire detection using the NOAA-series satellites," Washington, DC, NOAA, Tech. Rep. NESDIS 7, 1984.
[11] D. Huntley, "On the detection of shallow aquifers using thermal infrared imagery," *Water Resour. Res.*, vol. 14, pp. 1075-1083, 1978.
[12] M. A. Fosberg, C. D. Craig, and M. P. Waters III, "Application of infrared data from a geosynchronous meteorological satellite in surface wind modeling," in *Proc. Conf. Fire Forest Meteorol.*, vol. 6, pp. 265-275, 1980.
[13] M. J. Frampton and D. Marks, "Mapping snow surface temperature from thermal satellite data in the southern Sierra Nevada," in *Proc. Western Snow Conf.*, vol. 48, pp. 88-96, 1980.
[14] J. Dozier and S. G. Warren, "Effect of viewing angle on the infrared brightness temperature of snow," *Water Resour. Res.*, vol. 18, no. 5, pp. 1424-1434, 1982.
[15] M. Settle, "Current trends and research challenges in land remote sensing," in *Proc. Alpbach Summer School.* Noordwijk, Netherlands: European Space Agency, 1983.
[16] J. C. Price, "Land surface temperature measurements from the split window channels of the NOAA 7 advanced very high resolution radiometer," *J. Geophys. Res.*, vol. 89, pp. 7231-7237, 1984.
[17] H. Mannstein, "Surface energy budget, surface temperature and thermal inertia," in *Remote Sensing Applications in Meteorology and Climatology*, R. A. Vaughan, Ed., NATO ASI Ser. C: Math. Phys. Sci., vol. 201. Dordrecht, Netherlands: D. Reidel, 1987.
[18] P. J. Sellers, F. G. Hall, G. Asrar, D. E. Strebel, and R. E. Murphy, "The first ISLSCP field experiment (FIFE)," *Bull. Amer. Meteorol. Soc.*, vol. 69, no. 1, pp. 22-27, 1988.
[19] EOSAT/NASA Thermal-Infrared Working Group, *Commercial Applications and Scientific Research Requirements for Thermal-Infrared Observations of Terrestrial Surfaces.* Lanham, MD: Earth Observ. Sat. Co., 1986.
[20] D. Anding and R. Kauth, "Estimation of sea surface temperature from space," *Remote Sensing Environ.*, vol. 1, pp. 217-220, 1970.
[21] C. Prabakhara, G. Dalu, and V. G. Kunde, "Estimation of sea surface temperature from remote sensing in the 11- to 13-μm window region," *J. Geophys. Res.*, vol. 79, pp. 5039-5044, 1973.
[22] P. Y. Deschamps and T. Phulpin, "Atmospheric correction of infrared measurements of sea surface temperature using channels at 3.7, 11, and 12 μm," *Boundary-Layer Meteorol.*, vol. 18, pp. 131-143, 1980.
[23] R. L. Bernstein, "Sea surface temperature estimation using the NOAA 6 satellite Advanced Very High Resolution Radiometer," *J. Geophys. Res.*, vol. 87, no. C12, pp. 9455-9465, 1982.
[24] A. E. Strong and E. P. McClain, "Improved ocean surface temperatures from space-comparisons with drifting buoys," *Bull. Amer. Meteorol. Soc.*, vol. 65, pp. 139-142, 1984.
[25] E. P. McClain, W. G. Pichel, C. C. Walton, Z. Ahmad, and J. Sutton, "Multichannel improvements to satellite-derived global sea surface temperatures," *Adv. Space Res.*, vol. 2, pp. 43-47, 1983.
[26] M. P. Weinreb and M. L. Hill, "Calculation of atmospheric radiances and brightness temperatures in infrared window channels of satellite radiometers," Washington, DC, NOAA, Tech. Rep. NESS 80, 1980.
[27] F. X. Kneizys *et al.*, "Atmospheric transmittance/radiance: Computer code LOWTRAN6," Air Force Geophys. Lab., Bedford, MA, Rep. AFGL-TR-83-0187, 1983.
[28] M. T. Chahine, "Remote sounding of cloudy atmospheres, II, Multiple cloud formations," *J. Atmos. Sci.*, vol. 34, pp. 744-757, 1977.
[29] J. Susskind, J. Rosenfield, D. Reuter, and M. T. Chahine, "Remote sensing of weather and climate parameters from HIRS2/MSU on TIROS-N," *J. Geophys. Res.*, vol. 89, no. D3, pp. 4677-4697, 1984.
[30] F. Becker, "The impact of spectral emissivity on the measurement of land surface temperature from a satellite," *Int. J. Remote Sensing*, vol. 8, no. 10, pp. 1509-1522, 1987.
[31] M. Griggs, "Emissivities of natural surfaces in the 8- to 14-micron spectral region," *J. Geophys. Res.*, vol. 73, pp. 7545-7551, 1968.
[32] D. S. Kimes, "Azimuthal radiometric temperature measurements of wheat canopies," *Appl. Opt.*, vol. 7, pp. 1119-1121, 1981.
[33] J. Dozier, "A method for satellite identification of surface temperature fields of subpixel resolution," *Remote Sensing Environ.*, vol. 11, pp. 221-229, 1981.
[34] M. Matson and J. Dozier, "Identification of subresolution high temperature sources using a thermal IR sensor," *Photogram. Engrg. Remote Sens.*, vol. 47, pp. 1311-1318, 1981.
[35] S. Chandrasekhar, *Radiative Transfer.* New York: Dover, 1960.
[36] H. M. Nussenzveig and W. J. Wiscombe, "Efficiency factors in Mie scattering," *Phys. Rev. Lett.*, vol. 45, no. 18, pp. 1490-1494, 1980.
[37] W. J. Wiscombe, "Extension of the doubling method to inhomogeneous sources," *J. Quant. Spectrosc. Radiat. Transfer*, vol. 16, no. 6, pp. 477-489, 1976.
[38] ——, "The delta-M method: Rapid yet accurate radiative flux calculations for strongly asymmetric phase functions," *J. Atmos. Sci.*, vol. 34, pp. 1408-1422, 1977.
[39] I. P. Grant and G. E. Hunt, "Discrete space theory of radiative transfer, I, Fundamentals," in *Proc. Royal Soc. London*, vol. A313, pp. 183-197, 1969.
[40] W. J. Wiscombe, "On initialization, error and flux conservation in the doubling method," *J. Quant. Spectrosc. Radiat. Transfer*, vol. 16, pp. 635-658, 1976.
[41] S. Li, Z. Wan, and J. Dozier, "A component decomposition model for evaluating atmospheric effects in remote sensing," *J. Electromag. Waves Appl.*, vol. 1, no. 4, pp. 323-347, 1987.
[42] W. J. Wiscombe and J. W. Evans, "Exponential-sum fitting of radiative transmission functions," *J. Comput. Phys.*, vol. 24, pp. 416-444, 1977.
[43] D. S. Kimes, "View angle effects in the radiometric measurement of plant canopy temperatures," *Remote Sensing Environ.*, vol. 10, pp. 273-284, 1980.
[44] ——, "Remote sensing for row crop structure and component temperatures using directional radiometric temperatures and inversion techniques," *Remote Sensing Environ.*, vol. 13, pp. 33-55, 1983.
[45] M. Raffy and F. Becker, "An inverse problem occurring in remote sensing in the thermal infrared bands and its solution," *J. Geophys. Res.*, vol. 90, no. D3, pp. 5809-5819, 1985.
[46] T. Takashima and K. Masuda, "Emissivities of quartz and Sahara dust powders in the infrared region (7-17 μm)," *Remote Sensing Environ.*, vol. 23, pp. 51-63, 1987.
[47] R. A. Sutherland, "Broadband and spectral (2-18 μm) emissivity of some natural soils and vegetation," *J. Atmos. Oceanic Technol.*, vol. 3, pp. 199-202, 1986.
[48] EOSAT/NASA SeaWiFS Working Group, *System Concept for Wide-Field-of-View Observations of Ocean Phenomena from Space.* Lanham, MD: Earth Observ. Sat. Co., 1987.
[49] H. Jacobowitz and K. L. Coulson, "Effects of aerosols on the determination of the temperature of earth's surface from radiance measurements at 11.2 μm," Washington, DC, NOAA, Tech. Rep. NESS 66, 1973.
[50] A. E. Strong, "Monitoring El Chichón aerosol distribution using NOAA-7 satellite AVHRR sea surface temperature observations," *Geofisica Intl.*, vol. 23, no. 2, pp. 129-141, 1984.
[51] C. Walton, "Satellite measurement of sea surface temperature in the presence of volcanic aerosols," *J. Climate Appl. Meteorol.*, vol. 24, no. 6, pp. 501-507, 1985.
[52] L. M. McMillin and D. S. Crosby, "Theory and validation of the multiple window sea surface temperature technique," *J. Geophys. Res.*, vol. 89, no. C3, pp. 3655-3661, 1984.

*

Zhengming Wan received the B.A. degree in physics in 1965 from the Chinese University of Science and Technology, then located in Beijing. In 1979 he came to the Geography Department at the University of California, Santa Barbara, for graduate study, where he received the M.A. degree in 1981 and the Ph.D. degree in 1985.

He is now Associate Professor and Deputy Director at the Institute of Remote Sensing Applications of the Chinese Academy of Sciences in Beijing.

Jeff Dozier (M'86) received the B.A. degree in geography in 1968 from California State University, Hayward, and the M.Sc. and Ph.D. degrees in 1969 and 1973, respectively, from the University of Michigan, Ann Arbor.

He has taught since 1974 at the University of California, Santa Barbara, where he is now Professor of Geography and a Researcher in the Center for Remote Sensing and Environmental Optics. In 1987 he joined the Jet Propulsion Laboratory, California Institute of Technology, Pasadena, part-time, as Project Scientist for the High-Resolution Imaging Spectrometer (HIRIS), part of the Earth Observing System (Eos). His research interests are in remote sensing of snow properties, energy balance modeling of snow processes in alpine terrain, and snow chemistry and runoff.

Dr. Dozier serves as the U.S. National Representative to the International Commission on Snow and Ice (ICSI) and on two committees of the National Academy of Sciences: the Committee on Glaciology and the Committee on Opportunities in the Hydrologic Sciences. In 1987 he spent several months as a Visiting Scientist at NASA Headquarters.